Damage Detection for Port Infrastructure by Means of Machine-Learning-Algorithms

Frederic HAKE, Matthias HERMANN, Hamza ALKHATIB, Christian HESSE, Karsten HOLSTE, Georg UMLAUF, Gaël KERMARREC, and Ingo NEUMANN, Germany

Key words: Damage Detection; Multibeam echosounder; Laser scanning; Machine-Learning; Infrastructure

SUMMARY

The ageing infrastructure in ports requires regular inspection. This inspection is currently carried out manually by divers who sense by hand the entire underwater infrastructure. This process is cost-intensive as it involves a lot of time and human resources. To overcome these difficulties, we propose to scan the above and underwater port structure with a Multi-Sensor-System, and -by a fully automated process- to classify the obtained point cloud into damaged and undamaged zones.
We make use of simulated training data to test our approach since not enough training data with corresponding class labels are available yet. To that aim, we build a rasterised heightfield of a point cloud of a sheet pile wall by cutting it into verticall slices. The distance from each slice to the corresponding line generates the heightfield.
This latter is propagated through a convolutional neural network which detects anomalies. We use the VGG19 Deep Neural Network model pretrained on natural images. This neural network has 19 layers and it is often used for image recognition tasks. We showed that our approach can achieve a fully automated, reproducible, quality-controlled damage detection which is able to analyse the whole structure instead of the sample wise manual method with divers. The mean true positive rate is 0.98 which means that we detected 98 % of the damages in the simulated environment.-

Damage Detection for Port Infrastructure by Means of Machine-Learning-Algorithms

Frederic HAKE, Matthias HERMANN, Hamza ALKHATIB, Christian HESSE, Karsten HOLSTE, Georg UMLAUF, Gaël KERMARREC, and Ingo NEUMANN, Germany

1 MOTIVATION

The ageing infrastructure of sea and inland ports in Germany require new technologies and methods in the preparation and implementation of life cycle management. The previously personnel- and time-intensive work processes are being replaced by new automated, smart and innovative measurement and analysis processes to ensure transparency, resource efficiency and reliability.
Port infrastructure is subject to severe degradation over their lifetime due to human activities and environmental influences. Especially the material of seaports is profoundly affected by the saltwater. This causes structural damages to the concrete structures, sheet pile walls or wooden structures. In order to ensure the safety and stability of the infrastructure, it is crucial to detect and categorize the importance of the damage. Identifying structural damage in time allows early maintenance measures to be taken and can prevent costly repairs or even a collapse of the infrastructure

Monitoring of port infrastructural buildings is divided into two parts: above and underwater. The structural testing of port infrastructure above water is carried out by manual and visual inspections. The recording and documentation of the condition of damage underwater involve considerably more effort; the infrastructure is tested sample wise every 50 to 100 m; the divers slide down the structure and try to sense the wall with their hands. Human sensory tests and damage inspections underwater with divers are, therefore, highly variable in quality and quantity. Damage classification and -development is not reproducible due to the subjective perception. Furthermore, there is normally no comprehensive inspection underwater, which means that only a few percent of the structure can be inspected.
Therefore, a comprehensive building inspection in short time intervals is necessary. Due to the high amount of sediment, especially in the Ems, Weser and Elbe regions, a quality-controlled visual inspection is nearly impossible.
This study deals with a fully automated, quality-controlled and reproducible above and underwater 3D-Sensing and - damage-detection of port infrastructure: This is done usually using pattern recognition methods in modern data processing (see Hesse et al., 2019 for more information).
The results obtained in this way are to be used by the port operator to make the maintenance concepts and construction work following the building inspection transparent and reliable. This approach will reduce the downtimes of the port facilities and cost-intensive changes in the construction process significantly.
For the acquisition of building geometry and condition, not only exact, but also high-resolution 3D data for the underwater and above-water parts of the building are required. This

is the only way to reliably record damage and, based on this, to make a well-founded assessment of the current state of the structure.
In our system three different sensor types are merged into one kinematic-Multi-Sensor-System (k-MSS) for this detection task: a high-resolution hydroacoustic underwater multibeam echosounder, an above-water profile laser scanner and five HDR cameras. In addition to the IMU-GPS/GNSS method known from various applications, hybrid referencing with automatically tracking total stations is used for positioning (Figure 1). Although the individual sensors record in a grid pattern, the resulting point cloud is not grid-shaped due to the movements of the carrier platform.

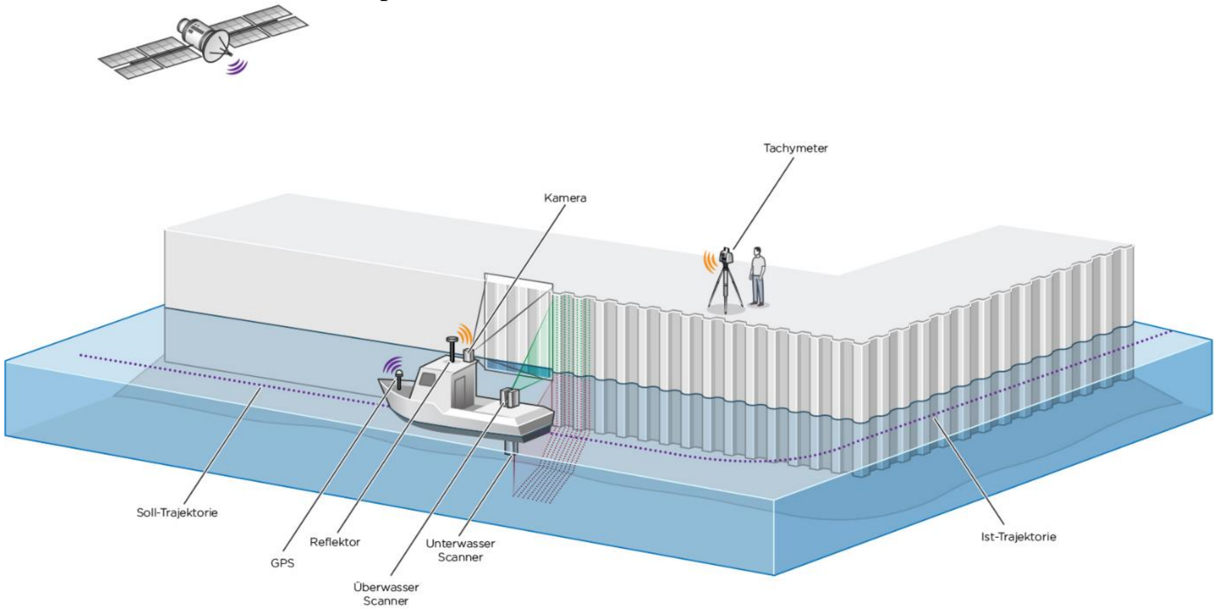

Figure 1: 3D recording of a port facility above and below water. (Hesse et al., 2019)

In this study we focus on geometrical damages since we are using only pointcloud data and no images from the cameras.
Various publications deal with comprehensive sensing methods for structural health monitoring for concrete or other materials above water or in clear offshore regions. Hadavandsiri et al. (2019) introduced a new approach for automatic, preliminary detection of damage in concrete structures with terrestrial ground scanners and a systematic threshold. O'Byrne et al. (2013) are detecting disturbances by texture segmentation of colour images. Gatys et al. (2015) showed that neural networks trained on natural images learn to represent textures in a way that enables synthesizing realistic textures and even whole scenes. Neural networks, as feature extraction are, thus, preferred over hand-crafted features (Yosinski et al., 2014; Carvalho et al., 2017 and Abati et al., 2019).
However, the limitation of such a transfer of features remains an open research question, especially when the input domain has the same topological structure, but different statistical structure.
In this work, we want to detect damages in point clouds. Therefore, we transfer features learnt from natural images to height maps from a range sensor. A heightmap or heightfield in computer graphics is a raster image that is mainly used as a discrete global grid in secondary height modeling. Each pixel records values, such as surface elevation data. In contrast to

natural images, the statistics of heightmaps depends on scan-resolution and the scanned object itself, which makes transferability difficult. A way to overcome this drawback is to train heightmap neural networks from scratch (Simony et al., 2018). The novelty detection approach we use can classify defective from non-defective features in a simulated data environment. This opens the door for further research in the use of pre-trained neural networks for range sensor data.

2 Related Work

Automated inspection of surfaces is always in favour to replace difficult, subjective or repetitive manual inspection processes. Three different approaches to automated inspection are reffered to in the literature (Kumar, 2008): 1. specifying a defect model and searching for similar patterns (Bodnarova et al., 1998), 2. looking for differences to a given reference template (Boracchi et al., 2014), and 3. learn discriminating between defects and non-defects (Racki et al., 2018)

Depending on available datasets, existing visual inspection approaches can be divided into two categories: supervised classification and novelty detection. When labelled samples of both defects and non-defects can be easily obtained, supervised classification approaches are preferred (Sarkar et al., 2018).

In practical applications only partial labelled data or strongly unbalanced data is available. In the context of defect detection, this means that either a large amount of defective data or non-defective data is available. Both situations massively complicate a supervised approach. Previous works, therefore, often make use of unsupervised learning techniques like novelty detection (Aiger & Talbot, 2012; Racki et al., 2018).

In novelty detection scenarios, only non-defective samples are considered during training. Such systems consist out of two in independent principle parts which are designed separately. The first part is a domain-specific feature extraction part, the second part is a general discriminator that judges novel samples (Miljković, 2010).

Earlier systems made use of handcrafted features based on, e.g., frequencies, interest points, sharp edges, or physical measures (Aiger & Talbot, 2012). Such features are powerful in specific situations with good domain knowledge and a small number of labelled data. However, general-purpose feature descriptors like SIFT (Lowe, 1999) are experimentally inferior to features extracted from neural networks (Nanni et al., 2017). Therefore modern systems often use features from a neural network in the first place before developing a specialized descriptor (Abati et al., 2019; Carvalho et al., 2017; Gatys et al., 2015 and Racki et al., 2018). Foremost, the particular neural network needs to be trained on a domain very similar to the operating domain (Yosinski et al., 2014). The obtained vector space is called feature space (Hastie et al., 2009).

The design of the discriminator is very flexible and very specific to the actual task. Some systems use a simple threshold, and others estimate areas of high density in feature space, various compress the information and measure reconstruction error. Any combinations of these are possible, too. Please refer to Miljković, 2010 or Pimentel et al., 2014 for a good overview of the existing method for classifying novelties.

The proposed method addresses such situations where only a few labelled defective data is available, and the most of the data is non-defective. Such methods learn a model based on non-defective reference data to discriminate between unseen defective and non-defective examples.

3 METHODOLOGY

To that aim, we start with a point cloud of typical harbour structures and firstly transform it into a heightfield which is described in chapter 3.1. Secondly in chapter 3.2, we extract features with a convolutional neural network. The third step is the defect detection by Local Outlier Factors (LoF) in chapter 3.3.

3.1 Heightfield generation

Input variables for the machine learning approach are rasterised distances between the point cloud and the original damage-free structure. In an optimal scenario, one can use a CAD- or BIM-model and determine deviations between model and point cloud. Unfortunately, no models are available for most existing port infrastructural buildings: to face this challenge, two possibilities exist: generation of an approximated surface or making use of a local moving-window approach.

In this study, we chose this latter approach and cut the point cloud into vertical slices of 5 cm in width. Each slice is approximated with a straight line using principal component analyses (PCA) (Jolliffe, 1986). The distances of each point to the line are then rasterised into a 2D heightfield with 2 cm raster size. The raster size depends resolution of the pointcloud and must be adapted to the respective data set. Empty cells, which occur due to data gaps or inappropriate point distribution, are interpolated with natural neighbour interpolation to avoid interferences in the feature extraction step. The whole process is implemented in MATLAB and Python and is summarized in a flowchart form in Figure 2.

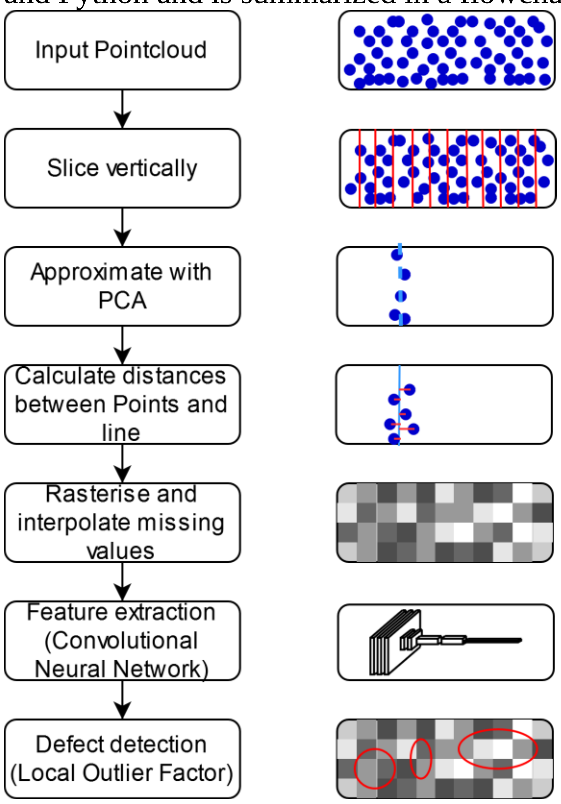

Figure 2: Flow chart of the automatic damage detection process

The obtained heightfield of the port infrastructure is interpreted as a scalar function defined on a 2d grid, denoted by $\boldsymbol{H}(\boldsymbol{x}, \boldsymbol{y})$. Afterwards, patches are extracted from the grid and flattened to data vectors. The data vectors $\boldsymbol{x}$ are organized as matrix $\boldsymbol{X}$ with shape $\boldsymbol{N} \times \boldsymbol{p}$, where $\boldsymbol{N}$ is the number of patches and $\boldsymbol{p}$ the number of pixels. Figure 3 shows an example of such an heightfield in pseudocolour. The data is further normalized by subtracting column-wise mean and scaling the column vectors to have unit variance (so-called standard normalization).

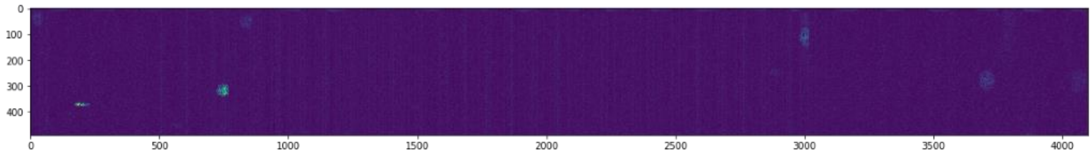

Figure 3: Visualizing an example heightfield on a 2d grid in pseudocolour.

3.2 Feature extraction

For extracting features, we use the VGG19 neural network (cf. Figure 4), a standard convolutional neural network (CNN) pretrained on natural images (Wan et al., 2020; Simonyan & Zisserman, 2014).The network consists of 19 layers and is trained in a classification scenario. It is well-known for achieving superhuman performance on the extensive scale image database ImageNet (http://www.image-net.org) consisting out of more than a million labelled natural images. We only keep the first convolutional layers of the network, i.e. including layer *pool_4*. It is interesting to note that deeper layers tend to learn higher-order characteristics (e.g. faces or objects) than lower layers (e.g. edges and structures). See Zeiler and Fergus (2014) for a comprehensible visualization.

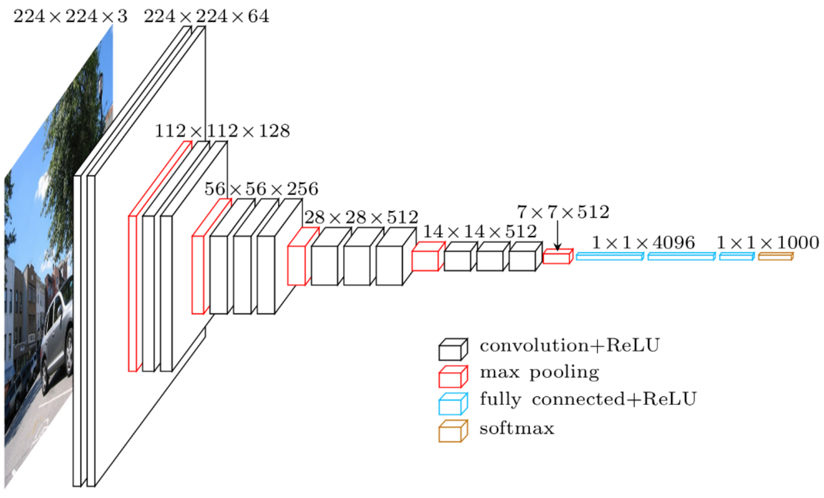

Figure 4: The layer architecture of the VGG19 network. Pooling layers are highlighted in red. (Simonyan & Zisserman, 2014).

In contrast to the scalar function of the heightfield, the VGG19 network expects three-channel RGB-colour input. To fulfil this requirement we broadcast the signal over three channels.

Every vector $\boldsymbol{x_I}$ is propagated through the network, and the intermediate activation of the *j*th layer is stored. Afterwards, the Gramian matrix of each activation is computed (see Gatys et al., 2015 for details). For computational efficiency and because we are not interested in synthesizing new data, we only keep the diagonal of the Gramian matrix, which relates to the energy per feature. This leads to the feature vector $\boldsymbol{z} \in \boldsymbol{R^k}$, where $\boldsymbol{k}$ is the number of feature maps in the *j*th layer of the network. Note that this procedure always leads to a dimensionality $\boldsymbol{k}$ independent of the input size $\boldsymbol{p}$. Again, we organize all feature vectors as rows in a matrix, resulting in feature matrix $\boldsymbol{Z}$ with shape $\boldsymbol{N} \times \boldsymbol{k}$.

3.3 Detection

As discriminator, the proposed method uses a standard approach called LoF (Breunig et al., 2000). This method constructs a reachability graph in feature space and derives an outlier score from this graph. This score is then used for threshold-based classification of new data. We denote the outlier score as $o_i = LoF(z_i)$, with $o_i \in R$. The threshold is derived from data. A new data point x_i is classified as a defect if its outlier score $o_i = LoF(\phi(x_i))$ is above the threshold t or as non-defect otherwise.

4 APPLICATIONS AND SIMULATION

Using a machine learning approach requires a large set of labelled training data. For the generation of a simulated point cloud of a sheet pile wall with damages, three steps are necessary:

1. Generation of a large number of datasets with randomly located and sized damages with a mathematical model for a sheet pile wall.
2. Computation of Cartesian coordinates of each point on the planes of the sheet pile wall by projecting rays from the k-MSS in vertical increments. The third dimension results from the movement of the sensor along a given trajectory. For the sake of simplicity, we used a straight line with equidistant sensor positions in this study.
3. Addition of a random number of damages onto the planes of the sheet pile wall. Each damage has an ellipsoidal shape with random values for the principal axis.

The result is noise-free point cloud. The ranges of each ray are then corrupted with random instrumental measurement uncertainty. The distance measurement uncertainty is assumed to be normally distributed and set according to the manufacturer´s specifications to 20 mm. The resulting resolution of the pointcloud is around 2 cm. Figure 5 illustrates the simulation procedure.

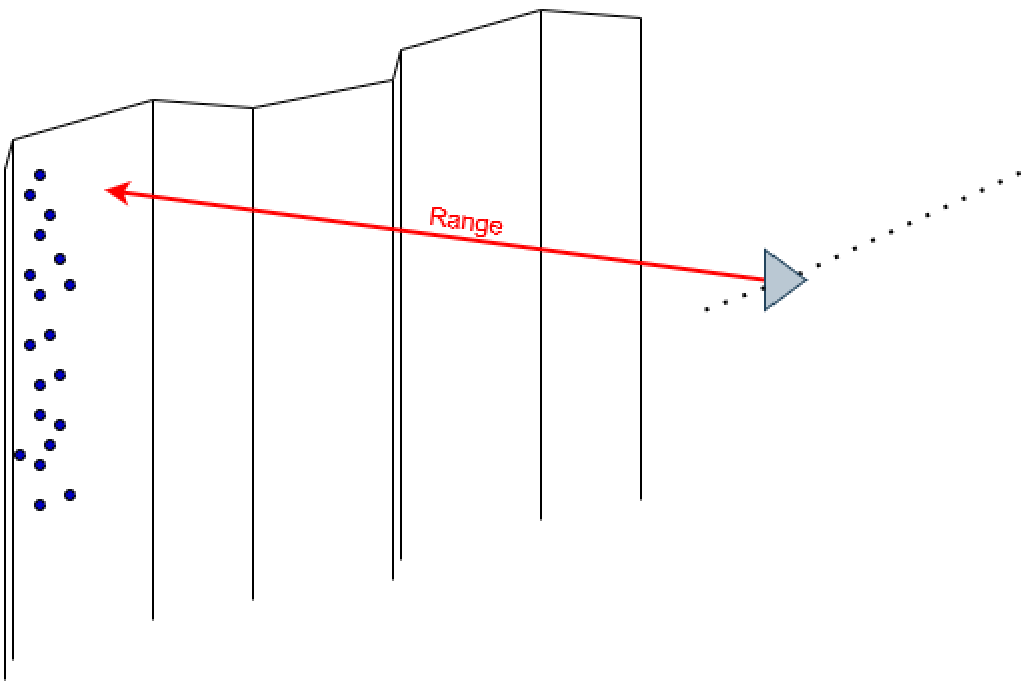

Figure 5: Simulation principal used in this study: at each sensor position, all rays in vertical increments according to the manufacturer´s specifications are intersected with the planes of the sheet pile wall.

A second dataset was generated: it indicates for every position whether it is damage or not and is thus the ground truth. Since the heightfield is a 2D raster image for the anomaly detection, we also use a 2D binary label image where one stands for damage and zero for non-damaged zones.
The label image is a 2D-raster with two classes representing damage or no damage (Figure 6 right). The raster is generated in the XZ-Plane of the point cloud. To avoid coarse shapes or misclassified raster cells, the image is filtered with the morphological operator's erosion and dilation (Serra, 1983). Erosion is used to separate two near clusters, and dilation fills small holes. Using erosion after dilation is also called opening in mathematical morphology. Figure 6 right shows the simulated point cloud with the corresponding label image.

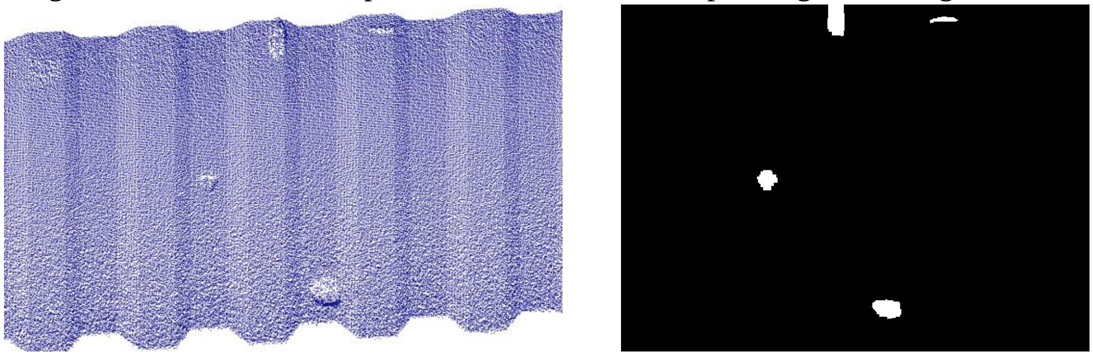

Figure 6: Left is the simulated point cloud and right the corresponding label map, where white stands for damage and black is no damage.

5 Evaluation

In our experiment, we use a patch size of 50×50 pixels which corresponds to $1\ m^2$ in world coordinates. The patches are extracted by a sliding window and have an overlap of 25 pixels. Note that no defect segmentation inside a patch is conducted — the whole patch is either defective or non-defective. Throughout experiments, we report average precision ratio (APR) and area under the curve (AUC) of receiver operating characteristics (ROC) (Schubert et al., 2012). Further, we keep 10 % of the training data as validation data X_{val} for deriving thresholds. The threshold t is chosen such that none of the M validation data vectors is classified as defective. Hence, the threshold is $t = max(\{o_1, \dots, o_M\})$. Further, the threshold is used to compute true-positive-rate (TPR), false-positive rate (FPR) and false-negative-rate (FNR). Results are averaged over 10 runs with different splits of validation and training data. In total there are 10 synthetic heightfields of the port infrastructure. The results of using two different sets of features are shown in Table 1 and Table 2. Table 1 shows the performance metrics of features taken from layer *pool_4*. As deeper layer tend to learn higher-order features it is interesting to see that the method has issues with the samples #1, #2 and #3.

Table 1: Results with activations (512d features) from layer pool_4 (numbers in braces correspond to number of training samples, number of non-defective test samples and number of defective test samples).

Heightfield no.	AUC	APR	TPR	FPR	FNR	TNR
#1	0.94±0.00	0.83±0.01	0.65±0.05	0.11±0.11	0.02±0.00	0.99±0.01
#2	0.93±0.00	0.79±0.01	0.53±0.09	0.05±0.02	0.06±0.01	0.99±0.00
#3	0.99±0.00	0.94±0.00	0.89±0.00	0.08±0.03	0.01±0.00	0.99±0.00
#4	1.00±0.00	1.00±0.00	1.00±0.00	0.13±0.08	0.00±0.00	0.98±0.01
#5	1.00±0.00	1.00±0.00	0.97±0.03	0.04±0.05	0.00±0.00	1.00±0.01
#6	1.00±0.00	1.00±0.00	0.97±0.03	0.19±0.06	0.00±0.00	0.99±0.00

Table 2 shows the results using features from the lower layer *pool_2*. It is easy to see that the overall detection performance is much better compared to the features from *pool_4*. Besides the feature hierarchy (i.e. feature order) there is another essential difference between layers of a CNN, which is scale. Every pooling operation reduces signal resolution and simultaneously increases the receptive field on the input. It follows that every layer is sensitive to patterns at a particular scale.

Table 2: Results with activations (128d features) from layer pool_2 (numbers in braces correspond to the number of training samples, number of non-defective test samples and number of defective test samples).

Heightfield no.	AUC	APR	TPR	FPR	FNR	TNR
#1	1.00±0.00	0.99±0.00	0.98±0.03	0.25±0.16	0.00±0.00	0.98±0.01
#2	1.00±0.00	0.99±0.00	0.93±0.02	0.07±0.04	0.01±0.00	0.99±0.00
#3	1.00±0.00	1.00±0.00	1.00±0.01	0.04±0.05	0.00±0.00	1.00±0.00
#4	1.00±0.00	1.00±0.00	1.00±0.00	0.12±0.10	0.00±0.00	0.98±0.01
#5	1.00±0.00	1.00±0.00	1.00±0.00	0.05±0.04	0.00±0.00	0.99±0.00
#6	1.00±0.00	1.00±0.00	1.00±0.00	0.04±0.05	0.00±0.00	1.00±0.00

As shown in Table 1, the mean TPR for activations with 512*d* features is 0.7, which means that 70 % of the damages are detected. Heightfield #1 and #2 are conspicuous due to their poorer value for TPR of 0.65 for #1 and 0.53 for #2. The mean FPR is 0.1, which is not very critical, but it should be decreased in future studies in terms of efficiency and cost reduction since a diver has to check every suspected case. The mean FNR is 0.02, and the mean TNR is 0.99 which means that 99 % of the no defective area has been classified correctly and only 0.02 % of the damages could not be detected.
The mean TPR for activations with 128*d* features, as shown in Table 2 is 0.98, and the mean FPR is 0.09 which indicates that 98 % of the damages are correctly classified and only 9 % non-defective area is misclassified. Conspicuous is heightfield #1 with a FPR of 0.25. The mean FNR is 0.001 which is very good since only 0.1 % are incorrectly classified, and the mean TNR is 0.99. That indicates that 99 % of the area is correctly classified as no damage. Overall the activations with 128*d* features seem to perform better on the synthetic datasets. This is also visible in table 3 and 4, which show the confusion matrices of the mean values. Figure 7 shows an example for the detected true positives in heightfield #6.

Table 3: Confusion matrix with activations (512d features) from layer pool_4.

0.70	0.1
0.02	0.99

Table 4: Confusion matrix with activations (128d features) from layer pool_2.

0.98	0.09
0.001	0.99

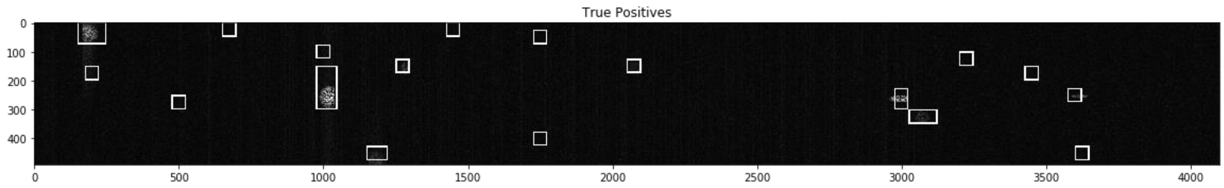

Figure 7: Detected true positives in heightfield #6.

6 CONCLUSION AND OUTLOOK

With the introduced method, the building inspection can be digitized and raised to a completely new level. With the used k-MSS, we achieve a significant higher completeness of the port inspections compared to the manual method with divers. By using laserscanner and hydrographic measurements, we obtain a quality-controlled and reproducible recording of the infrastructure. Due to the area-based measurement of the component surfaces above and underwater, suspected damage can be reliably detected and verified. A comparison of different measurement epochs - as they have to be carried out every six years within the framework of structural inspections - is thus also possible for underwater constructions, so that the development of damage and the service life of these constructions, which are important for our national economy, can be better observed and evaluated in future. With the introduced approach to use heightfields as input for constitutional neural networks we achieve a fully automated damage detection. The mean true positive rate is 0.98 for the activation (128*d* features) from layer *pool_2* for simulated data.

The lack of enough training data forced us to use simulated data only for this study. The first results show a high potential of the introduced method. But the performance can vary for real data.

Next studies should focus on performing the algorithms on real data and optimising control variables. Therefore, this approach should be applied to real-world data in different conditions and locations.

Acknowledgement

This work was supported by the Federal Ministry of Education and Research (grant number: 13N14540) and by the Federal Ministry of Transport and Digital Infrastructure (grant number: 19H18011C).

IHATEC Innovative Hafentechnologien

Gefördert durch:

Bundesministerium für Verkehr und digitale Infrastruktur

aufgrund eines Beschlusses des Deutschen Bundestages

7 REFERENCES

Abati, D., Porrello, A., Calderara, S., & Cucchiara, R. (2019). Latent Space Autoregression for Novelty Detection. In *The IEEE Conference on Computer Vision and Pattern Recognition (CVPR)*.

Aiger, D., & Talbot, H. (2012). The phase only transform for unsupervised surface defect detection. In *Emerging Topics In Computer Vision And Its Applications* (pp. 215–232). World Scientific.

Bodnarova, A., Bennamoun, M., & Kubik, K. K. (1998). Defect detection in textile materials based on aspects of the HVS. In *SMC'98 Conference Proceedings. 1998 IEEE International Conference on Systems, Man, and Cybernetics (Cat. No. 98CH36218).* Symposium conducted at the meeting of IEEE.

Boracchi, G., Carrera, D., & Wohlberg, B. (2014). Novelty detection in images by sparse representations. In *2014 IEEE Symposium on Intelligent Embedded Systems (IES).* Symposium conducted at the meeting of IEEE.

Breunig, M. M., Kriegel, H.-P., Ng, R. T., & Sander, J. (2000). LOF: identifying density-based local outliers. In *Proceedings of the 2000 ACM SIGMOD international conference on Management of data*.

Carvalho, T., Rezende, E. R. S. de, Alves, M. T. P., Balieiro, F. K. C., & Sovat, R. B. (2017). Exposing computer generated images by eye's region classification via transfer learning of VGG19 CNN. In *2017 16th IEEE International Conference on Machine Learning and Applications (ICMLA).* Symposium conducted at the meeting of IEEE.

Gatys, L., Ecker, A. S., & Bethge, M. (2015). Texture synthesis using convolutional neural networks. In *Advances in neural information processing systems*.

Hadavandsiri, Z., Lichti, D. D., Jahraus, A., & Jarron, D. (2019). Concrete Preliminary Damage Inspection by Classification of Terrestrial Laser Scanner Point Clouds through Systematic Threshold Definition. *ISPRS International Journal of Geo-Information*, *8* (12), 585. https://doi.org/10.3390/ijgi8120585

Hastie, T., Tibshirani, R., & Friedman, J. (2009). *The elements of statistical learning: data mining, inference, and prediction*. Springer Science & Business Media.

Hesse, C., Holste, K., Neumann, I., Hake, F., Alkhatib, H., Geist, M., Knaack, L., & Scharr, C. (2019). 3D HydroMapper: Automatisierte 3D-Bauwerksaufnahme und Schadens-erkennung unter Wasser für die Bauwerksinspektion und das Building Information Modelling. *Hydrographische Nachrichten-Journal of Applied Hydrography* (113), 26–29.

Jolliffe, I. T. (1986). Principal components in regression analysis. In *Principal component analysis* (pp. 129–155). Springer.

Kumar, A. (2008). Computer-vision-based fabric defect detection: A survey. *IEEE Transactions on Industrial Electronics*, *55* (1), 348–363.

Lowe, D. G. (1999). Object recognition from local scale-invariant features. In *Proceedings of the seventh IEEE international conference on computer vision.* Symposium conducted at the meeting of IEEE.

Miljković, D. (2010). Review of novelty detection methods. In *The 33rd International Convention MIPRO.* Symposium conducted at the meeting of IEEE.

Nanni, L., Ghidoni, S., & Brahnam, S. (2017). Handcrafted vs. non-handcrafted features for computer vision classification. *Pattern Recognition*, *71*, 158–172.

O'Byrne, M., Schoefs, F., Ghosh, B., & Pakrashi, V. (2013). Texture analysis based damage detection of ageing infrastructural elements. *Computer-Aided Civil and Infrastructure Engineering*, *28* (3), 162–177.
Pimentel, M. A.F., Clifton, D. A., Clifton, L., & Tarassenko, L. (2014). A review of novelty detection. *Signal Processing*, *99*, 215–249. https://doi.org/10.1016/j.sigpro.2013.12.026
Racki, D., Tomazevic, D., & Skocaj, D. (2018). A compact convolutional neural network for textured surface anomaly detection. In *2018 IEEE Winter Conference on Applications of Computer Vision (WACV)*. Symposium conducted at the meeting of IEEE.
Sarkar, K., Hampiholi, B., Varanasi, K., & Stricker, D. (2018). Learning 3d shapes as multi-layered height-maps using 2d convolutional networks. In *Proceedings of the European Conference on Computer Vision (ECCV)*.
Schubert, E., Wojdanowski, R., Zimek, A., & Kriegel, H.-P. (2012). On Evaluation of Outlier Rankings and Outlier Scores. In J. Gosh, H. Liu, I. Davidson, C. Domeniconi, & C. Kamath (Eds.), *Proceedings of the 2012 SIAM International Conference on Data Mining* (pp. 1047–1058) [Society for Industrial and Applied Mathematics]. https://doi.org/10.1137/1.9781611972825.90
Serra, J. (1983). *Image analysis and mathematical morphology*. Academic Press, Inc.
Simony, M., Milzy, S., Amendey, K., & Gross, H.-M. (2018). Complex-YOLO: An Euler-Region-Proposal for Real-time 3D Object Detection on Point Clouds. In *The European Conference on Computer Vision (ECCV) Workshops*.
Simonyan, K., & Zisserman, A. (2014, September 4). *Very Deep Convolutional Networks for Large-Scale Image Recognition*. http://arxiv.org/pdf/1409.1556v6
Wan, X., Liu, L., Wang, S., & Wang, Y. (2020). A Transfer Learning Strip Steel Surface Defect Recognition Network Based on VGG19. In Y. Wang, K. Martinsen, T. Yu, & K. Wang (Eds.), *Lecture Notes in Electrical Engineering: v. 634. Advanced manufacturing and automation IX* (Vol. 634, pp. 333–341). Springer. https://doi.org/10.1007/978-981-15-2341-0_41
Yosinski, J., Clune, J., Bengio, Y., & Lipson, H. (2014). How transferable are features in deep neural networks? In Z. Ghahramani, M. Welling, C. Cortes, N. D. Lawrence, & K. Q. Weinberger (Eds.), *Advances in Neural Information Processing Systems 27* (pp. 3320–3328). Curran Associates, Inc. http://papers.nips.cc/paper/5347-how-transferable-are-features-in-deep-neural-networks.pdf
Zeiler, M. D., & Fergus, R. (2014). Visualizing and Understanding Convolutional Networks. In D. Fleet, T. Pajdla, B. Schiele, & T. Tuytelaars (Eds.), *Computer Vision - ECCV 2014* (pp. 818–833). Springer International Publishing.

CONTACTS

Frederic Hake M.Sc. Geodetic Institute Leibniz University Hannover Nienburger Str. 1 30167 Hannover GERMANY Tel. +49 5117624469 Email: hake@gih.uni-hannover.de Web site: www.gih.uni-hannover.de	Matthias Hermann M.Sc. Institute for Optical Systems University of Applied Sciences Konstanz Alfred-Wachtel-Straße 8 78462 Konstanz GERMANY Tel. +49 7531206619 Email: Matthias.Hermann@htwg-konstanz.de Web site: www.ios.htwg-konstanz.de
Dr.-Ing. Hamza Alkhatib Geodetic Institute Leibniz University Hannover Nienburger Str. 1 30167 Hannover GERMANY Tel. +49 5117622468 Email: alkhatib@gih.uni-hannover.de Web site: www.gih.uni-hannover.de	Dr.-Ing. Christian Hesse Dr. Hesse und Partner Ingenieure Veritaskai 6 21079 Hamburg GERMANY Tel. +49 40522991900 Email: ch@dhpi.com Web site: www.dhpi.com
Dipl.-Ing. (FH) Karsten Holste WKC Hamburg GmbH Veritaskai 8 21079 Hamburg GERMANY Tel. +49 407900010 Email: Karsten.Holste@wk-consult.com Web site: www.wk-consult.com	Prof. Dr. Georg Umlauf Institute for Optical Systems University of Applied Sciences Konstanz Alfred-Wachtel-Straße 8 78462 Konstanz GERMANY Tel. +49 7531206702 Email: umlauf@htwg-konstanz.de Web site: www.ios.htwg-konstanz.de
Dr. Gaël Kermarrec Geodetic Institute Leibniz University Hannover Nienburger Str. 1 30167 Hannover GERMANY Tel. +49 51176214763 Email: kermarrec@gih.uni-hannover.de Web site: www.gih.uni-hannover.de	Prof. Dr.-Ing. Ingo Neumann Geodetic Institute Leibniz University Hannover Nienburger Str. 1 30167 Hannover GERMANY Tel. +49 5117622461 Email: neumann@gih.uni-hannover.de Web site: www.gih.uni-hannover.de